LBL-30584
Preprint

Lawrence Berkeley Laboratory
UNIVERSITY OF CALIFORNIA

Materials & Chemical Sciences Division

Submitted to Physical Review B

Surface Structure of $\sqrt{3}x\sqrt{3}$ R30° Cl/Ni(111) Determined Using Low-Temperature Angle-Resolved Photoemission Extended Fine Structure

L.-Q. Wang, Z. Hussain, Z.Q. Huang, A.E. Schach von Wittenau,
D.A. Shirley, and D.W. Lindle

April 1991

LOAN COPY
Circulates
for 4 weeks
Bldg. 50 Library.
LBL-30584
Copy 2

Prepared for the U.S. Department of Energy under Contract Number DE-AC03-76SF00098

DISCLAIMER

This document was prepared as an account of work sponsored by the United States Government. Neither the United States Government nor any agency thereof, nor The Regents of the University of California, nor any of their employees, makes any warranty, express or implied, or assumes any legal liability or responsibility for the accuracy, completeness, or usefulness of any information, apparatus, product, or process disclosed, or represents that its use would not infringe privately owned rights. Reference herein to any specific commercial products process, or service by its trade name, trademark, manufacturer, or otherwise, does not necessarily constitute or imply its endorsement, recommendation, or favoring by the United States Government or any agency thereof, or The Regents of the University of California. The views and opinions of authors expressed herein do not necessarily state or reflect those of the United States Government or any agency thereof or The Regents of the University of California and shall not be used for advertising or product endorsement purposes.

Lawrence Berkeley Laboratory is an equal opportunity employer.

DISCLAIMER

This document was prepared as an account of work sponsored by the United States Government. While this document is believed to contain correct information, neither the United States Government nor any agency thereof, nor the Regents of the University of California, nor any of their employees, makes any warranty, express or implied, or assumes any legal responsibility for the accuracy, completeness, or usefulness of any information, apparatus, product, or process disclosed, or represents that its use would not infringe privately owned rights. Reference herein to any specific commercial product, process, or service by its trade name, trademark, manufacturer, or otherwise, does not necessarily constitute or imply its endorsement, recommendation, or favoring by the United States Government or any agency thereof, or the Regents of the University of California. The views and opinions of authors expressed herein do not necessarily state or reflect those of the United States Government or any agency thereof or the Regents of the University of California.

Surface Structure of $\sqrt{3}x\sqrt{3}$ R30° Cl/Ni(111) Determined Using Low-Temperature Angle-Resolved Photoemission Extended Fine Structure

Li-Qiong Wang, Z. Hussain, Z.Q. Huang, A.E. Schach von Wittenau,
and D.A. Shirley

Department of Chemistry, University of California
and Materials and Chemical Sciences Division
Lawrence Berkeley Laboratory, 1 Cyclotron Road
Berkeley, California 94720

D.W. Lindle
National Institute of standards and Technologies, Gaithersburg, Maryland 20899

This work was supported by the Director, Office of Energy Research, Office of Basic Energy Sciences, Chemical Sciences Division of the U.S. Department of Energy under Contract No. DE-AC03-76SF00098.

Abstract

A surface structural study of the $\sqrt{3}x\sqrt{3}$ R30° Cl/Ni(111) adsorbate system was made using low-temperature Angle-Resolved Photoemission Extended Fine Structure (ARPEFS). The experiments were performed along two emission directions, [111] and [110], and at two temperatures, 120 K and 300 K. The Multiple-Scattering Spherical-Wave (MSSW) analysis determined that the Cl atom adsorbs in the fcc three-fold hollow site, 1.837 (8) Å above the first nickel layer, with a Cl-Ni bond length of 2.332 (6) Å, and an approximate 5% contraction between the first and the second nickel layers (the errors in parentheses are statistical standard deviations only).

I. Introduction

Adsorbed atoms or molecules frequently cause relaxations of substrate surfaces. However, the understanding of adsorbate-induced substrate surface relaxation requires accurate and detailed surface and near-surface structural information. Angle-resolved photoemission extended fine structure (ARPEFS)[1-5] has proven to be a powerful tool in this regard.

ARPEFS is the angle-resolved and energy-dependent form of photoelectron diffraction due to the final-state interference between the direct and the scattered photoelectron waves.[6] Fourier transformation of the extended fine structure provides direct and qualitative structural information. However, the more quantitative structural analysis requires Multiple-Scattering Spherical-Wave (MSSW) theory.[7] With a MSSW level analysis, effects as subtle as small corrugation and relaxation near the substrate surface can be characterized. Because thermal effects (larger mean-square-relative atomic displacements) reduce the amount of structural information present in the fine structure, cooling the lattice effectively extends the range of ARPEFS to deeper layers. Recent studies[5,8] have shown that the adsorbate geometry and the substrate relaxation can be determined more accurately by using low-temperature ARPEFS. In this paper, we employ low-temperature ARPEFS to study the $\sqrt{3}x\sqrt{3}$ R30° Cl/Ni(111) system.

There are several published reports of structural studies of halogen atoms on metal surfaces. For example, the c(2×2) Cl/Cu(001) system has been studied by several groups.[5,9-11] However, there are few studies of halogen atoms on fcc (111) surfaces. In SEXAFS study of $\sqrt{3}x\sqrt{3}$ R30° Cl/Cu(111), D.P. Woodruff et al.[12] were unable to obtain accurate distances beyond the first-nearest neighbors, or to distinguish the two different three-fold hollow adsorption sites of the fcc (111) surface. However, these two inequivalent hollow sites were distinguished in their photoelectron diffraction study, where only the distance from Cl to the first substrate layer was given. Since ARPEFS has high directional sensitivity, the different substrate atoms can be emphasized by choosing different emission geometries. Thus, ARPEFS can clearly distinguish between two kinds of three-fold adsorption sites. In our study, we use low-temperature ARPEFS

to determine the adsorption site as well as to obtain an accurate distance to the second substrate layer for the $\sqrt{3}x\sqrt{3}$ R30° Cl/Ni(111) system. Interestingly, H. Kuroda et al.[13] recently reported a study of the same Cl/Ni(111) system using combination of SEXAFS and the x-ray standing-wave method. They found that no substrate surface relaxations in the $\sqrt{3}x\sqrt{3}$ R30° Cl/Ni(111), as opposed to the p(2x2)S/Ni(111)[14] where a significant contraction of 15 % was observed with respect to the bulk spacing. Thus, their study offers an opportunity to compare the structural results obtained from different techniques.

This paper is organized as follows. Section II gives the experimental details and the procedures of data collection and reduction. Section III describes two types of analysis: Fourier and multiple-scattering analysis, and present results. Section IV discusses and compares the results. A summary and conclusions are given in section V.

II. Experimental

The experiments were performed on Beamline X24A[15] at the National Synchrotron Light Source at Brookhaven using a Ge(111) double-crystal monochromator. The Cl 1s photoemission spectra were taken in the kinetic energy range from 50 to 550 eV, with photon energies from 2870 to 3370 eV. The resolution of the double-crystal monochromator was approximately 1 eV through this photon energy range. Data were collected with a rotatable hemispherical electrostatic analyzer[16] which has the energy resolution of ~ 1 eV FWHM under the operating conditions of 160 eV pass energy, and the angular resolution of the input lens of ± 3°. The experimental chamber was equipped with a four-grid LEED/Auger systems, an ion gun, and an effusive beam doser for introducing chlorine gas.

A nickel single crystal was cut, oriented to within ± 1° of the (111) direction as determined by Laue backscattering, then mechanically polished and chemically etched. Since the fcc (111) crystal lacks two-fold symmetry, it is hard to tell the crystal azimuthal orientation from the p(1x1) LEED pattern. Thus, several Laue pictures were taken at different x-ray incident directions along

the fixed crystal axis to define the azimuthal orientation of the crystal. The final finished crystal was attached to a Ta sample plate mounted on a high-precision manipulator with a liquid nitrogen cooling system. Sample heating was accomplished by electron bombardment from a tungsten filament located behind the sample plate. The temperatures were measured by a chromel-alumel thermocouple attached to the sample plate next to the sample. The nickel crystal was cleaned by repeated cycles of Ar^+ ion sputtering and annealing to about 880 K. This procedure was sufficient to remove all impurities except carbon. Carbon was then removed by heating the crystal to 770 K after exposure to $1x10^{-8}$ torr of oxygen for several minutes. The crystal was taken as clean when AES showed no detectable traces of carbon, nitrogen, oxygen, or sulfur contamination and a sharp p(1x1) LEED pattern was observed. The chamber pressure was about $3x10^{-10}$ torr during measurements. Because chlorine exposure to a clean Ni(111) surface produces a sequence of LEED patterns with superstructures, and a sharp $\sqrt{3}x\sqrt{3}$ R30° LEED pattern is stable within a relatively small exposure range corresponding to ~ 0.2 L, the $\sqrt{3}x\sqrt{3}$ R30° Cl overlayer preparation was done carefully in several steps. A sharp $\sqrt{3}x\sqrt{3}$ R30° Cl overlayer LEED pattern was produced by dosing Cl_2 through an effusive beam doser at room temperature for a total of 4-5 minutes with the main chamber pressure at ~ $1x10^{-9}$ torr. This was followed by a 350 K annealing for two minutes to dissociate Cl_2 completely into atomic Cl.

The experiments were carried out along two emission directions, [111] and [110], and at two temperatures, 120 ± 5 K and 300 K. These four sets of ARPEFS data were taken on separately prepared samples. The sample was flashed to about 350 K every 6-9 hrs during data collection, and more often for the low-temperature measurements. The crystal orientation angle for each geometry was determined by a He-Ne laser autocollimation through the experimental chamber viewports with an accuracy of ± 2°. The experimental geometries are shown in Fig. 1. For the normal [111] geometry, photoelectrons were collected along the surface normal with the photon polarization vector 35° from the surface normal toward the $[11\bar{2}]$ direction, while for the offnormal [110] geometry, the emission direction and photon polarization vector are co-linear along the [110] direction. These two geometries were chosen to highlight nearby backscattering atoms, utilizing

the directional sensitivity of ARPEFS. The [111] geometry can determine interlayer spacings effectively, while the [110] geometry was selected to emphasize the nearest-neighbors along the [110] direction.

For each emission geometry at a given temperature, a series of photoemission spectra was collected over a 50-550 eV kinetic energy range in equal electron wave-number increments of 0.08 $Å^{-1}$. Each photoemission spectrum was centered on the Cl 1s photoelectron peak, with an energy window of 25 - 30 eV. The experimental background consisted of three photoemission scans covering the kinetic energy range of 40-560 eV. Each scan was taken at a different photon energy so that the Cl 1s photoemission peak lay about 10 eV below the lowest kinetic energy in each spectrum. This experimentally measured background was used in the least-square fitting for the normalization of each photoemission spectrum to compensate for the inhomogeneous photon flux and the electron analyzer transmission function. The photoemission intensity was extracted by least-square fitting of each photoemission spectrum with three functions: a Voigt function to model the core-level photoelectron peak, a Gaussian convoluted with a step function (G step) to describe the inelastically-scattered electrons associated with the photoelectron peak, and an experimentally-measured background to account for other inelastic scattering processes. The detailed procedures have been described previously.[5]

In analogy to EXAFS, the total normalized photoemission intensity I(E) as a function of kinetic energy E is composed of a slowly varying atomic-like portion and a rapidly oscillating contribution due to the interference effects of electron scattering from neighboring ion cores. I(E) can be described as:

$$I(E) = [\chi(E) + 1]\, I_0(E) \quad , \qquad (1)$$

where $I_0(E)$ is a slowly varying atomic-like function and $\chi(E)$ is the oscillatory interference function which can be determined by removing the slowly varying function $I_0(E)$ from the total photoemission intensity I(E):

$$\chi(E) = \frac{I(E) - I_0(E)}{I_0(E)} \quad . \qquad (2)$$

The experimental $\chi(E)$ curves are shown in Fig. 2 for the [111] and [110] data at two temperatures, 120 K and 300 K, respectively. $I_0(E)$ was fitted with simple low-order polynomials for constructing $\chi(E)$ curves. We can see from Fig. 2 that the oscillation amplitudes of $\chi(E)$ at the lower temperature are enhanced as compared with those at room temperature. The oscillation patterns are matched well at the two temperatures.

For Fourier data analysis, it is necessary to convert $\chi(E)$ to $\chi(k)$. The photoelectron kinetic energy E measured outside the solid is related to the wave-number k of the photoelectron inside the solid by the De Broglie relation:

$$k = \hbar^{-1}\sqrt{2m_e\,(E + V_0)}\ , \qquad (3)$$

where m_e is the electron rest mass and V_0 is the inner potential of the solid. The value of V_0 is typically about 10 eV, but the exact value is unknown. The V_0 is therefore treated as an adjustable parameter in the fits.

III. Analysis and Results

Structural information can be extracted from the experimental $\chi(k)$ curves in two ways: by Fourier analysis and by Multiple-Scattering Spherical-Wave (MSSW) analysis. We first treat the data by Fourier analysis to obtain qualitative structural information such as adsorption site and approximate geometric parameters. MSSW calculations are then required to obtain quantitative structural information.

A. Fourier Analysis

Using the single-scattering model of ARPEFS[6], the expression for $\chi(k)$ can be written as

$$\chi(k) = 2\sum_j \frac{\cos\beta_j}{\cos\gamma}\frac{|f(\theta_j)|}{R_j} e^{-\Delta R_j/\lambda} e^{-\sigma_j^2(1-\cos\theta_j)k^2} \cos[kR_j\,(1-\cos\theta_j) + \phi_j]\ . \qquad (4)$$

The summation is over all atoms near the adsorbed "source" atom from which core-level photoemission originates. Here β_j is the angle between the photon polarization vector and the vector connecting the emitting atom and the j th scattering atom, R_j is the distance from the photoemitter to the j th scattering atom, and γ is the angle between the emission direction and the photon polarization vector. The k-dependent complex scattering factor $f(\theta_j)$ for a given scattering angle θ_j can be divided into the magnitude $|f(\theta_j)|$ and the phase ϕ_j. The emission-angle dependent path-length difference is given by $\Delta R_j = R_j (1-\cos\theta_j)$. The temperature effect is introduced as a Debye-Waller factor, where σ_j is the Mean-Square Relative Displacement (MSRD) between the photoemitter and the j th scattering atom, projected on the photoelectron momentum change direction. Inelastic losses due to excitation of plasmons and electron-hole pairs by the energetic photoelectron are incorporated in an electron mean-free path λ.

The cosinusoidal dependence of the $\chi(k)$ function permits a Fourier transformation, yielding an amplitude spectrum peaked near various scattering path-length differences. Fourier spectra for the [111] and [110] data at the two temperatures are given in Fig. 3. V_0 value of 10 eV was used. Forward ($\theta_j = 0°$) and backward ($\theta_j = 180°$) scatterings give the strongest signals: the strong feature at a path-length difference ~ 4.6 Å in the [110] direction arises from a nearest-neighbor Ni atom located directly behind Cl along the [110] direction, at a Cl-Ni bond length of ~ 2.3 Å. Atop and bridge adsorption sites are excluded because they have no backscattering atom along the [110] direction to give the strong peak at ~ 4.6 Å. However, there are two different three-fold hollow adsorption sites, which are called the fcc and hcp sites, respectively. The fcc sites are directly above atoms in the third substrate layer, while the hcp sites are directly above atoms in the second substrate layer. Fig. 4 illustrates that one of the nearest-neighbor Ni atoms lies behind the Cl atom along the [110] direction in the fcc site, but not in the hcp site. Therefore, the strong Fourier backscattering peak in the [110] direction indicates that the fcc three-fold hollow site is the one occupied in the $\sqrt{3}x\sqrt{3}$ R30° Cl/Ni(111) system. Furthermore, the two peaks at ~ 7.6 Å and ~ 9.1 Å in the [110] direction can be attributed mainly to scattering from the atoms in the second Ni(110) plane, while the first peak at ~ 2.5 Å in the [110] direction, corresponds to

scattering from two nearest-neighboring atoms symmetrically located at either side of the plane containing the [111] and [110] directions.

Fourier spectra in the [111] direction show two peaks at ~ 3.9 Å and ~ 7.8 Å. The first peak is due to scattering from the three nearest-neighboring atoms in the first Ni layer, while the second peak corresponds to scattering from the three third-nearest neighbor atoms in the second Ni layer. Thus, the normal emission data suggest that we can determine the distance of Cl to both the first and second Ni layers, providing information about the substrate surface relaxation.

B. Multiple-Scattering Analysis

ARPEFS studies[1-5] have shown that the detailed quantitative geometric structures can be obtained by comparing experimental $\chi(k)$ curves with theoretical calculations based on Multiple-Scattering Spherical-Wave (MSSW) theory[7], which comprehensively describes the ARPEFS scattering process. The MSSW calculation requires as input both structural and non-structural parameters. The copper and chlorine phase shifts were available from previous calculations.[5,17-18] The mean free path was included in an exponential factor, $e^{-r/\lambda}$, with $\lambda = ck$ and $c = 0.75$. Thermal effects were treated using a correlated Debye model which included surface-layer dependent and anisotropic Mean-Square Relative Displacements (MSRD).[7] The nickel bulk Debye temperature was taken as 390 K, while the nickel surface Debye temperature was set to 276 K, which assumes that the surface nickel atoms have an MSRD twice as that of the bulk. The Debye temperature for the Cl overlayer was estimated to be 355 K from the nickel surface Debye temperature adjusted for the difference in masses. Surface Debye temperatures for both Cl and Ni were, however, varied in the calculations based on the above estimated values. In addition, the emission and polarization angles ($\pm 3°$), the experimental temperature (120 ± 10 K) and the inner potential (10 ± 5 eV) were allowed to vary in the calculations.

First, both the [111] and the [110] experimental $\chi(k)$ curves at the two temperatures were smoothed by Fourier filtering out the high-frequency portion of the data (path-length differences

larger than 10.0 Å). Thus, the cutoff at about 10.0 Å eliminates high-frequency noise and retains all the real signals from down to the second substrate layer. Also, the cutoffs below 1.8-2.0 Å were made due to uncertainties of the low frequency portion of the data. All subsequent comparisons of theory with experiment were done with the filtered data, 2.0-10.0 Å for the [111] data, and 1.8-10.0 Å for the [110] data. The MSSW calculations were performed with the same path-length difference cutoffs.

The fcc three-fold adsorption site had already been determined for the $\sqrt{3}x\sqrt{3}$ R30° Cl/Ni(111) system from the Fourier analysis above. Comparisons of the MSSW calculations with the experimental data confirm this result. The $\chi(k)$ curves for two different three-fold adsorption geometries (fcc and hcp) were calculated using the bulk Ni spacing (2.03 Å) with a Cl-Ni bond length of 2.3 Å estimated form the Fourier analysis. Fig. 5 shows the comparison of the calculated $\chi(k)$ curves with the experimental data for the [111] and [110] directions at 120 K, respectively. By visual inspection, the calculated curve in the [110] direction for the fcc site unambiguously resembles the experimental data more than that for the hcp site, while in the [111] direction, it is not clear which calculated $\chi(k)$ curve more closely resembles the experimental data. Since there is a backscattering atom near the photoemitter for the fcc site, but not for the hcp site in the [110] direction, the calculated $\chi(k)$ curve for the hcp site has rather different features and weaker amplitude as compared with that for the fcc site. Thus, MSSW calculations provide strong evidence to support the fcc three-fold site, consistent with the Fourier analysis. However, there are still large differences between the experimental $\chi(k)$ curve and the calculations for the fcc site using nonoptimized geometrical parameters. This suggests possible substrate surface relaxation in the $\sqrt{3}x\sqrt{3}$ R30° Cl/Ni(111) system.

To derive a detailed quantitative structure, we optimized both structural and nonstructural parameters to achieve the best agreement between the theory and the experiment. An R-factor (reliability-factor) was used as a quantitative measure of the fit between the experiment and the theory. The optimum geometrical parameters were obtained when a minimal R-factor defined by

$$R = \frac{\int[\chi_E(k) - \chi_T(k)]^2 dk}{\int \chi_T(k)^2 dk} , \qquad (5)$$

was reached. Here E and T denote experiment and theory. The R-factors were calculated over the k range 5.2-11.2 $Å^{-1}$.

In recent ARPEFS studies,[5,8] an automatic routine was successfully used to search many parameters simultaneously with a reasonable number of iterations. The detailed procedure of this routine has been described previously. No lateral substrate relaxation and no corrugation of the second substrate layer were considered because of the $\sqrt{3}x\sqrt{3}$ R30° structure of the Cl/Ni(111) system. The experimental data were fitted with two structural parameters: Cl-Ni(1), the vertical distance of Cl to first Ni layer, and Cl-Ni(2), the vertical distance of Cl to second Ni layer, while other nonstructural parameters such as electron emission angles, adsorbate and substrate surface Debye temperatures, the experimental temperature, and the inner potential were treated as adjustable parameters with reasonable initial guesses and bounds. The emission angles were found to be < 3° from the expected values for all the data sets. The inner potential for the optimum geometry was 10 ± 2 eV, and the experimental temperature was optimized to be 120 ± 5 K. R-factor minima lay in the small range R = 0.05 - 0.13 in the various calculations.

The structural parameters determined from the best fits are listed in Table I, with statistical errors in parentheses. The error associated with each parameter was estimated as described in our previous study.[5] The best fits of the MSSW calculations to the filtered (10.0Å) experimental $\chi(k)$ curves are shown in Figs. 6 and 7 for the [111] and [110] geometries at the two temperatures, respectively. Agreements between the theoretical and experimental curves are excellent. From Table I, we can see that the structural parameters obtained from the four data sets were consistent, especially for the data at different temperatures with a given geometry. There are larger errors for the Cl-Ni(2) parameter in the [110] direction than those in the [111] direction, showing different sensitivity of a given data set to each structural parameter due to the directional sensitivity of ARPEFS.

Fig. 8 shows R-factor plots for the [111] and the [110] geometries at the two temperatures, calculated by varying the Cl-Ni(1) and Cl-Ni(2) distances, respectively, while other parameters were fixed in their optimum values. The R-factor curvature for the Cl-Ni(2) distance in the [111] direction is steeper than that in the [110] direction, giving smaller error bars for the Cl-Ni(2) distance in the [111] geometry. Moreover, the R-factor minima were smaller for a given geometry at the lower temperature, due to the increased signal to noise ratio. The interlayer spacing between the first and the second Ni layers can thus be determined more accurately from the analysis of the low-temperature [111] data.

The top and side views of the $\sqrt{3}x\sqrt{3}$ R30° Cl/Ni(111) structure are shown in Fig. 4. From Table I, the Cl-Ni(1) distance of 1.837(8) Å gives a Cl-Ni bond length of 2.332(6) Å. The Cl-Ni(2) distance of 3.763(7) Å then yields interlayer spacing between the the first and the second Ni layers Ni(1)-Ni(2) of 1.926(11) Å, showing an approximate 5 % contraction from the bulk value of 2.03 Å.

IV. Discussion

The vertical distance of Cl to the first Ni layer Cl-Ni(1) of 1.837(8) Å obtained from this study is 0.08 Å smaller than the recent SEXAFS study[13] by Kuroda et al. This difference is beyond the standard error of each of the two techniques. However, studies on the p(2x2) S/Ni(111) system using several different techniques also showed rather different results for the vertical distance of S to the first Ni layer S-Ni(1), ranging from 1.40 to 1.66 Å.[14,19-22] For example, a SEXAFS study[14] by the same group gave the S-Ni(1) distance as 1.66 Å, while a LEED study[19] by Mitchell et al. showed a distance of 1.50 Å, a 0.16 Å difference. Furthermore, a recent low-temperature ARPEFS study[8] on the same system found the S-Ni(1) distance of 1.54 Å, which is closer to the LEED study. We can see that the distances of adsorbate to the first substrate layer from SEXAFS studies on both p(2x2) S/Ni(111) and $\sqrt{3}x\sqrt{3}$ R30° Cl/Ni(111) systems tend to be larger than the results obtained from LEED and ARPEFS studies. This suggests some sort of

unknown systematic errors among these techniques. With recent improvements in the quality of data and analysis, it now appears that ARPEFS, LEED, and SEXAFS may be inherently capable of yielding structural parameters of high precision: ± 0.01 - 0.02 Å in the case of ARPEFS, for example. If the remaining discrepancies among the three methods arise from systematic errors, the resolution of those errors is important.

The current ARPEFS study found a 0.104 Å or 5% contraction of the topmost Ni interlayer spacing as compared with that of the bulk for the $\sqrt{3}x\sqrt{3}$ R30° Cl/Ni(111) system by analyzing structural information from the first and the second Ni layers. However, Kuroda et al. reported no relaxation in the same Cl/Ni(111) system, in contrast to a significant contraction of 15 % in the p(2x2) S/Ni(111) system using their SEXAFS results combined with those from the x-ray standing-wave method. Fig. 9 shows the comparisons of the experimental data for both the [111] and the [110] geometries at 120 K with the calculated $\chi(k)$ curves based on the bulk Ni spacing (2.03 Å), while other parameters were kept fixed at their optimum values. By visual inspection, the agreements for both geometries are very poor, indicating that the substrate surface relaxation is required to obtain the best fits between the experiment and the theory shown in Figs. 6 and 7. Although a combination of x-ray standing-wave and SEXAFS studies provides direct information about the relaxation of the first substrate layer relative to the bulk position, the information about the topmost interlayer spacing is indirect, as it requires the second substrate layer to remain in the bulk position. Low-temperature ARPEFS itself, however, can obtain the topmost interlayer spacing directly for the $\sqrt{3}x\sqrt{3}$ R30° Cl/Ni(111) system, due to its ability to probe the second substrate layer.

Studies on the clean Cu(111) surface[23] showed a 0.7 ± 0.5% contraction of the topmost interlayer spacing, smaller than the contractions on more open (001) and (110) surfaces. If the clean Ni(111) surface also has little contraction in the topmost interlayer spacing, a 5% contraction in the $\sqrt{3}x\sqrt{3}$ R30° Cl/Ni(111) system is much larger than that of clean Ni(111) surface, indicating the adsorbate-induced contraction. In contrast to the Cl/Ni(111) system, studies of adsorbates on fcc (001) surfaces such as S- and Cl-covered Ni(001) and Cu(001) have shown expansions of the

topmost interlayer spacing,[1,5,8-11,24-25] which has been attributed to metal-metal bond weakening induced by adsorption. The mechanism for contraction is not clear in the $\sqrt{3}x\sqrt{3}$ R30° Cl/Ni(111) system.

The previous low-temperature ARPEFS study on the Cl/Cu(001) system showed that cooling the lattice effectively extends the range of ARPEFS to the fourth substrate layer.[5] However, in this study, we could only obtain the distances from Cl to the first and to the second layers. In Fig. 2, we note consistent high-frequency oscillations in the experimental $\chi(k)$ curves at two temperatures, as compared with the filtered (10 Å) curves shown in Figs. 6 and 7, suggesting the existence of real signals at large path-length differences (>10 Å). Fig. 10 shows the experimental Fourier spectrum in the [111] direction at 120 K, with the Fourier spectra obtained from single- and multiple-scattering calculations based on the optimized parameters. The agreement among these three Fourier transform spectra in the range 10 Å - 25 Å is not good enough to permit a quantitative structural interpretation, but it is intriguing. The single-scattering curve shows peaks spaced at 4 Å intervals, consistent with backscattering from the Ni(111) planes spaced at 2.03 Å. In fact, weak peaks near 20 Å and 24 Å, consistent with scattering from the fifth and sixth layers, appear in all three curves. However, for intermediate path-length differences 10 Å - 18 Å, single scattering yields only two peaks, while both multiple scattering and experiment show four. The later two curves agree only in regard to the overall intensity of the pattern of four peaks, but not with respect to their exact positions or detailed intensity pattern. We therefore conclude that the single-scattering calculation omits important (multiple-scattering) effects which show up in the experimental curve, and the multiple-scattering theory, as we have applied it, does not model these effects accurately.

V. Conclusion

We have presented a low-temperature ARPEFS study of the $\sqrt{3}x\sqrt{3}$ R30° Cl/Ni(111) system. The surface structure was determined by two methods: Fourier analysis which gives

qualitative structural information and the Multiple-Scattering Spherical-Wave (MSSW) analysis, which yields more quantitative results. This ARPEFS study provided a clear distinction between the two inequivalent three-fold hollow sites using directional sensitivity of ARPEFS and found that the fcc three-fold hollow site is favoured for the $\sqrt{3}x\sqrt{3}$ R30° Cl/Ni(111) system. Low-temperature ARPEFS allows us to determine structural parameters more accurately due to the increased signal-to-noise ratio. Multiple-Scattering Spherical-Wave (MSSW) analysis found the Cl atom adsorbed in the fcc three-fold hollow site, 1.837(8) Å above the first nickel layer with a Cl-Ni bond length of 2.332(6) Å and an approximate 5% contraction between the first and the second nickel layers, in disagreement with a recent study[13] by Kuroda et al.

Acknowledgment

This work was supported by the Director, Office of Energy Research, Office of Basic Energy Sciences, Chemical Sciences Division of the U.S. Department of Energy under Contract No. DE-AC03-76SF00098. The experiments were performed at the National Synchrotron Light Source at Brookhaven National Laboratory, which is supported by the U.S. Department of Energy's Office of Basic Energy Sciences. We are greatly indebted to J. Stohr for the loan of Ni(111) single crystal and to B. Karlin for providing the assistance in running the monochromator. Z. Hussain wishes to acknowledge KFUPM for the grant of a sabbatical leave.

Table I. Summary of the structural results (in Å) determined from MSSW analysis. The statistical errors associated with each parameter for the four data sets are given in parentheses.[5] The structural parameter values in the upper panel are derived directly from fits of the data, while those in the lower panel were derived by subtracting two corresponding values above the line.

Parameter	$[111]_{120k}$	$[111]_{300k}$	$[110]_{120k}$	$[110]_{300k}$	Avg[a] (stat)	Avg[b] (scat)	This work [c]
Cl-Ni(1)	1.831(8)	1.828(10)	1.848(9)	1.844(16)	1.837(5)	1.838(8)	1.837(8)
Cl-Ni(2)	3.767(10)	3.763(13)	3.754(14)	3.761(40)	3.763(7)	3.761(5)	3.763(7)
Cl-Ni (bond length)					2.332(4)	2.333(6)	2.332(6)
Ni(1)-Ni(2)					1.926(10)	1.923(9)	1.926(11)

a) Statistical errors only: Standard deviation.

b) Standard deviation from the scatter of results.

c) Final adopted values, with standard deviation taken as the higher of a and b above. Not included in these values and error estimate are any possible offset due to (unknown) systematic error.

Reference

1. J.J. Barton, C.C. Bahr, S.W. Robey, Z. Hussain, E. Umbach and D.A. Shirley, *Phys. Rev.* **B 34,** 3807 (1986).
2. S.W. Robey, J.J. Barton, C.C. Bahr, G. Liu and D.A. Shirley, *Phys. Rev.* **B 35,** 1108 (1987).
3. L.J. Terminello, X.S. Zhang, Z.Q. Huang, S. Kim, A.E. Schach von Wittenau, K.T. Leung and D.A. Shirley, *Phys. Rev.* **B 38,** 3879 (1988).
4. X.S. Zhang, L.J. Terminello, S. Kim, Z.Q. Huang, A E. Schach von Wittenau and D.A. Shirley, *J. Chem. Phys.* **89**, 6538 (1988).
5. L.Q. Wang, A.E. Schach von Wittenau, Z.G. Ji, L.S. Wang, Z.Q. Huang, and D.A. Shirley, (submitted to *Phys. Rev.* **B**).
6. J.J. Barton, C.C. Bahr, Z. Hussain, S.W. Robey, J.G. Tobin, L.E. Klebanoff and D.A. Shirley, Phys. *Rev. Lett.* **51**, 272 (1983).
7. J.J. Barton, S.W. Robey and D.A. Shirley, *Phys. Rev.* **B 34**, 778 (1986).
8. A.E. Schach von Wittenau, L.Q. Wang, Z.G. Ji, Z.Q. Huang, T. Shulman and D.A. Shirley (in preparation).
9. F. Jona, D. Westphal, A. Goldmann and P.M. Marcus, *J. Phys. C: Solid State Phys.* **16**, 3001 (1983).
10. P.H. Citrin, D.R. Hamann, L.F. Mattheiss and J.E. Rowe, *Phys. Rev. Lett.* **49**, 1712 (1982).
11. J.R. Patel, D.W. Berreman, F. Sette, P.H. Citrin and J.E. Rowe, *Phys. Rev.* **B 40**, 1330 (1989).
12. M.D. Crapper, C.E. Riley, P.J.J. Sweeney, C.F. McConville, D.P. Woodruff, and R.G. Jones, *Surf. Sci.* **182**, 213 (1987)
13. M. Funabashi, Y. Kitajima, T. Yokoyama, T. Ohta and H. Kuroda, *Physica* **B 158**, 664 (1989)
14. T. Yokoyama, M. Funabashi, Y. Kitajima, T. Ohta and H. Kuroda, *Physica* **B 158**,

643 (1989)

15. P.L. Cowan, S. Brennan, R.D. Deslattes, A. Henins, T. Jach, and E.G. Kessler, *Nucl. Instrum, Methods* **A 246**, 154(1986).
16. S.D. Kevan, Ph.D. thesis, University of California, Berkeley, 1980; LBL-11017.
17. P.J. Orders and C.S. Fadley, *Phys. Rev.* **B 27**, 781 (1983).
18. J.B. Pendry, Low Energy Electron Diffraction (Academic, London, 1974).
19. Y.K. Wu and K.A.R. Mitchell, *Can. J. Chem.* **67**, 1975 (1989).
20. T. Fauster, H. Durr, and D. Hartwig, *Surf. Sci.* **178**, 657 (1986).
21. D. R. Warburton, P.L. Wincott, G. Thornton, F.M. Quinn, and D. Norman, *Surf. Sci.* **211/212**, 71 (1989).
22. J.E. Demuth, D.W. Jepsen, and P.M. Marcus, *Phys. Rev. Lett* **32**, 1182 (1974).
23. S.A. Lindgren, L. Wallden, J. Rundgren and P. Westrin, *Phys. Rev.* **B 29**, 576 (1984).
24. J.E. Demuth, D.W. Jepsen, and P.M. Marcus, *Phys. Rev. Lett.* **31** 540 (1973), and **32**, 1184 (1974).
25. T. Yokoyama, Y. Takata, T. Ohta, M. Funabashi, Y. Kitajima, and H. Kuroda, *Phys. Rev.* **B 42**, 7000 (1990)

Figure Captions

FIG. 1. A view of the $\sqrt{3}x\sqrt{3}$ R30° overlayer of chlorine (shaded atoms) on the (111) face of a nickel single crystal. The emission directions are labelled as [111] and [110], while the photon polarization vectors associated with each geometry are labelled as $\hat{\varepsilon}_{[111]}$ and $\hat{\varepsilon}_{[110]}$, respectively.

FIG. 2. Experimental $\chi(k)$ curves for the [111] and the [110] geometries. The curve with solid dots is $\chi(k)$ at 300 K, and the heavier curve is $\chi(k)$ at 120 K.

FIG. 3. Fourier spectra for the [111] and the [110] geometries at two temperatures, 120 K and 300 K. The heavier curves are the spectra at 120 K.

FIG. 4. Top and side views of the $\sqrt{3}x\sqrt{3}$ R30° Cl/Ni(111) structure. The smaller shaded circles represent the Cl atoms in the fcc sites, while the smaller open circles represent the Cl atoms in the hcp sites. The side view (lower panel) corresponds to a cut in the plane shown the broken line in the top view (upper panel).

FIG. 5. Adsorption site determination for the [111] and the [110] geometries at 120 K. The experimental curves (solid lines) are compared to the MSSW calculated curves (dashed lines) for two kinds of unreconstructed three-fold hollow adsorption geometries (fcc and hcp).

FIG. 6. The best fits of the MSSW calculations (dashed curves) to the filtered (10.0 Å) ARPEFS data (solid curves) for the [111] geometry at two temperatures, 120 K and 300 K.

FIG. 7. The best fits of the MSSW calculations (dashed curves) to the filtered (10.0 Å) ARPEFS data (solid curves) for the [110] geometry at two temperatures, 120 K and 300 K.

FIG. 8. R-factor plots for the [111] and the [110] geometries at the two temperatures, 120 K and 300 K, calculated by varying the Cl-Ni(1) and the Cl-NI(2) distances, respectively, while other parameters were fixed in their optimum values.

FIG. 9. Comparisons of the filtered (10.0 Å) ARPEFS data (solid curves) to the MSSW calculations (dashed curves) for the [111] and [110] geometries at 120 K. The MSSW curves are calculated with the bulk Ni spacing (2.03 Å), while all the other parameters are kept fixed at their optimum values.

FIG. 10. Comparison among the Fourier spectra for the [111] geometry at 120 K: experimental Fourier spectrum with those spectra obtained from single- and multiple-scattering calculations based on the optimized parameters.

$\sqrt{3} \times \sqrt{3}$ R30° Cl/Ni(111)

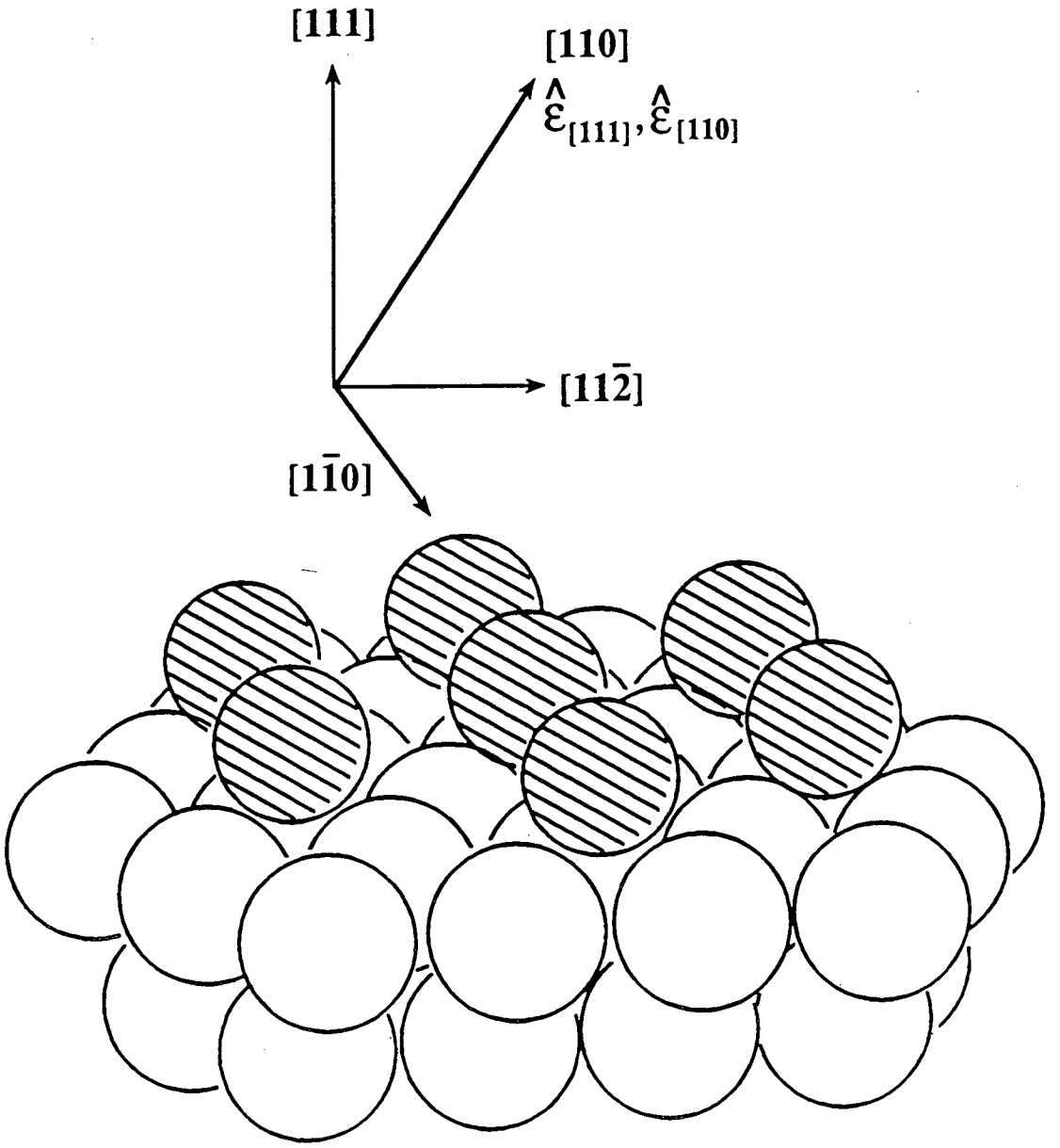

XBL 914-738

Fig.(1)

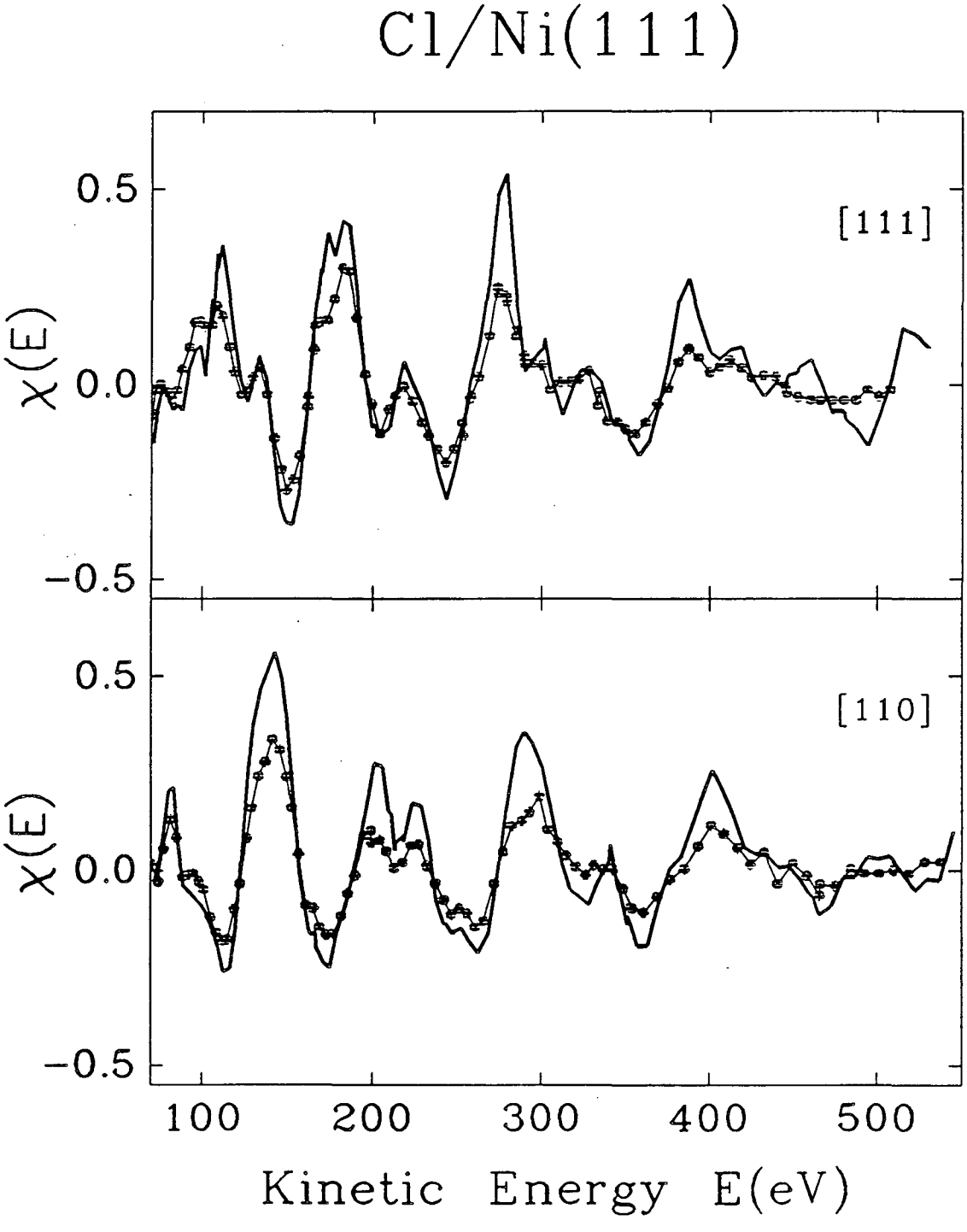
Cl/Ni(111)
[111]
[110]
χ(E)
0.5
0.0
−0.5
100
200
300
400
500
Kinetic Energy E(eV)

Fig.(2)

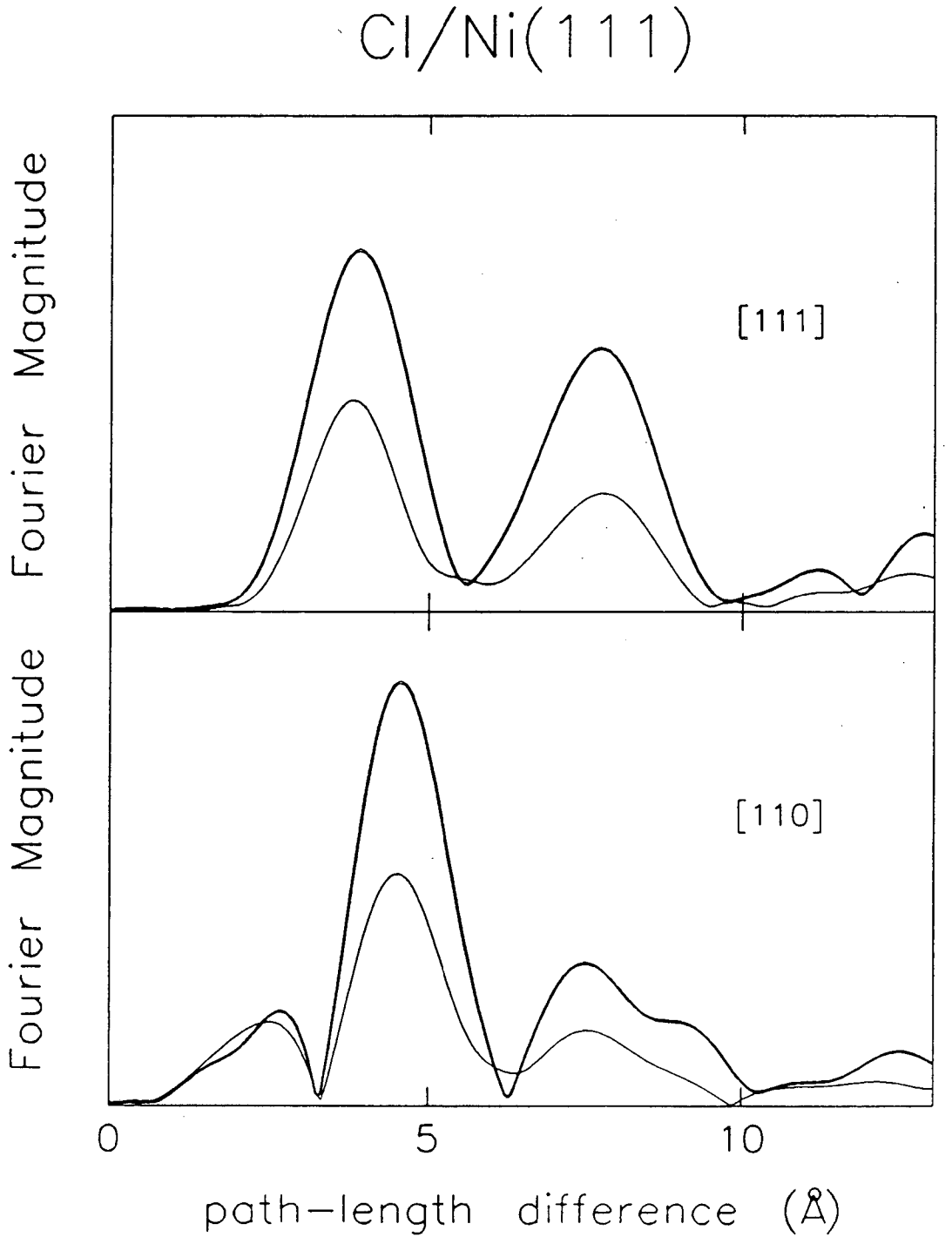
Cl/Ni(111)
Fourier Magnitude
[111]
Fourier Magnitude
[110]
0
5
10
path-length difference (Å)

Fig.(3)

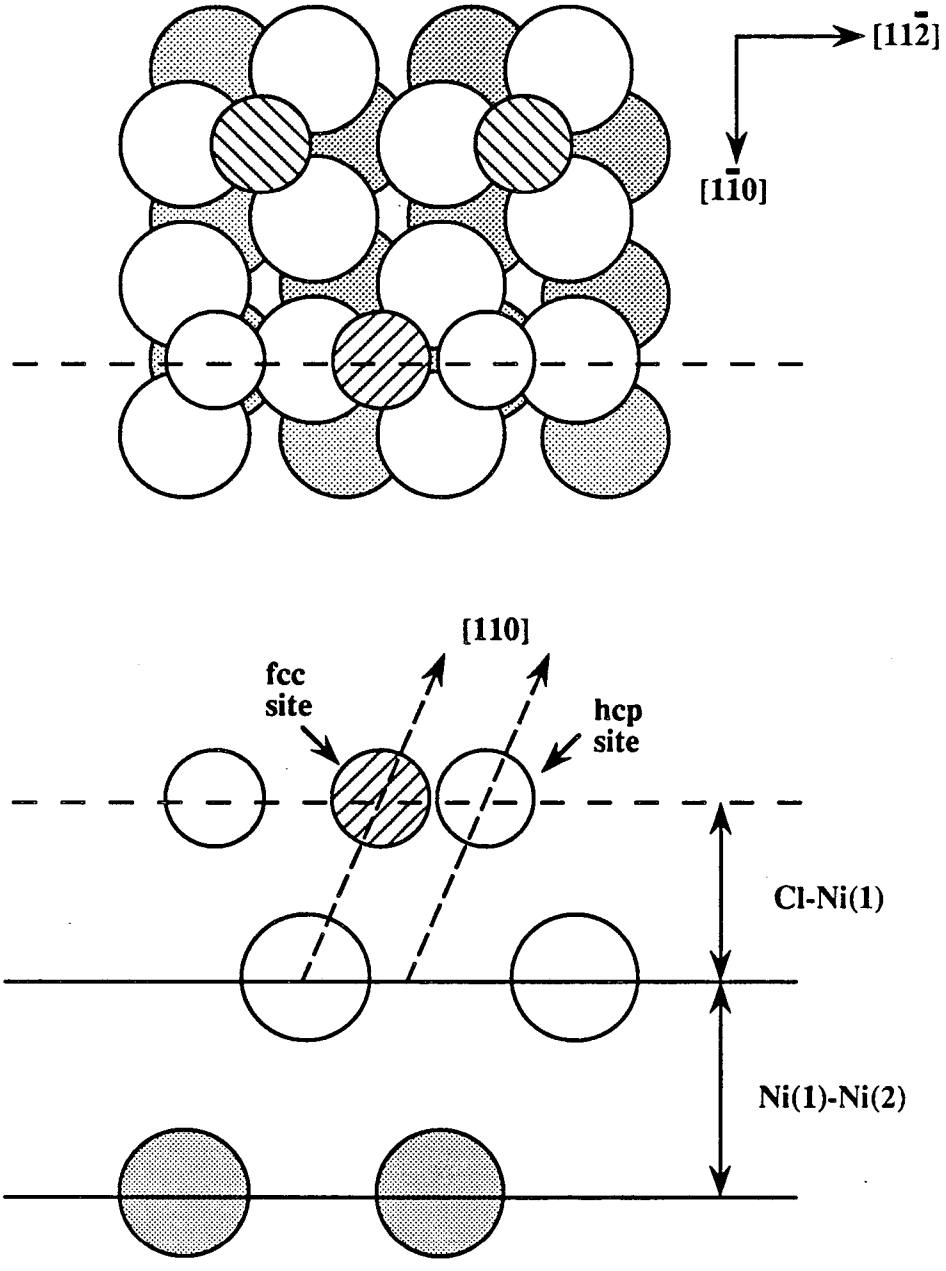

Fig.(4)

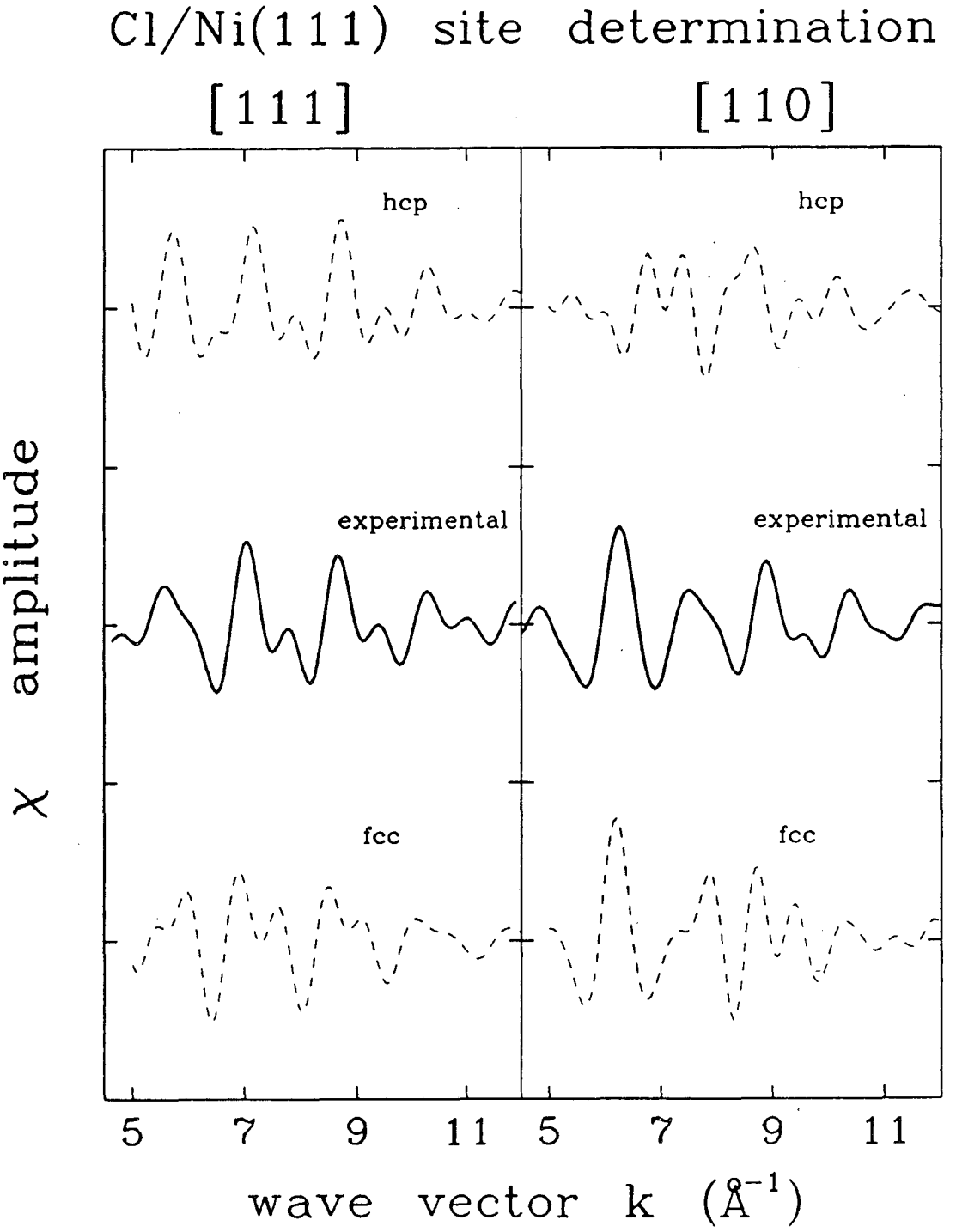
Cl/Ni(111) site determination
[111]
[110]
hcp
hcp
experimental
experimental
fcc
fcc
χ amplitude
5
7
9
11
5
7
9
11
wave vector k (Å^{-1})

Fig.(5)

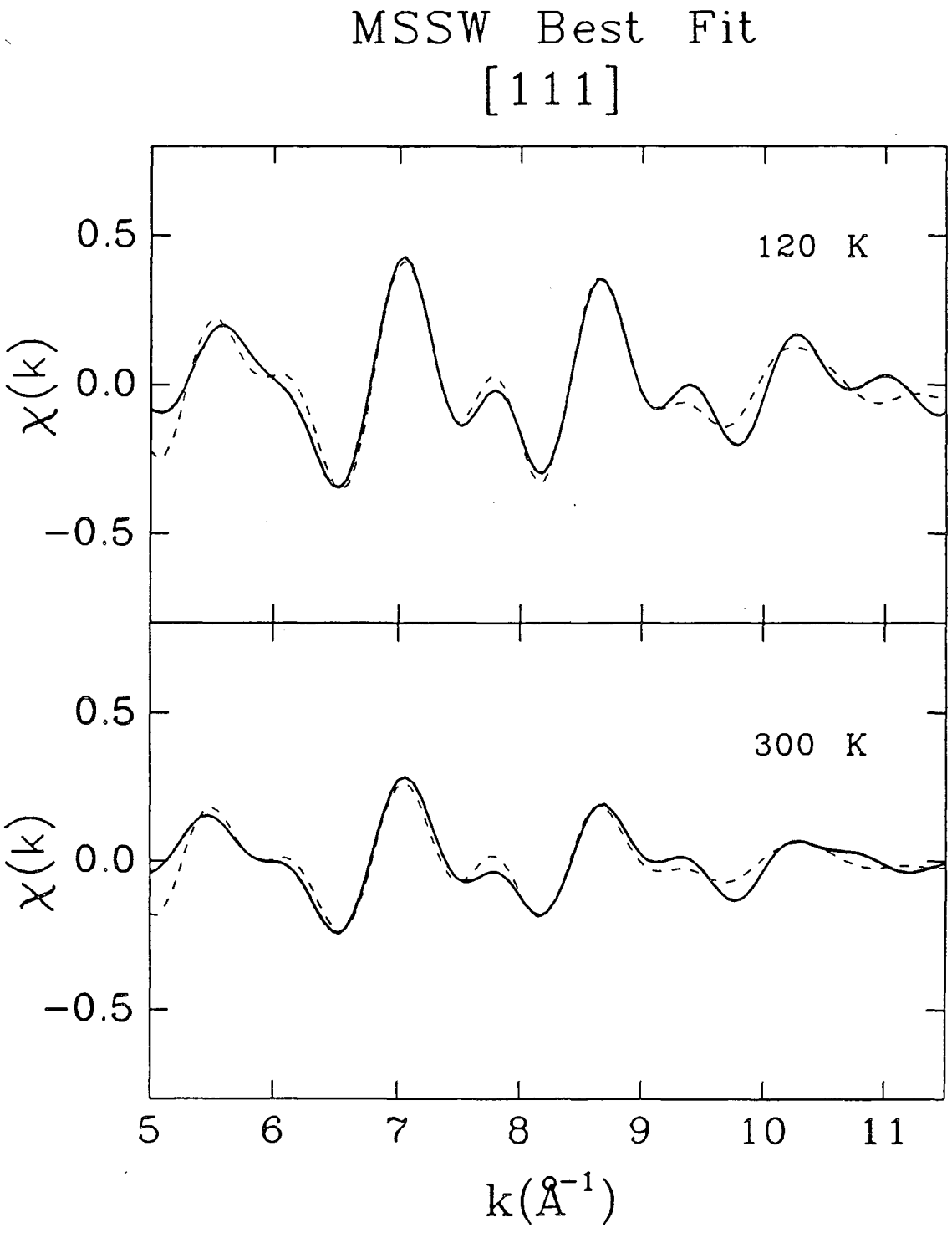

Fig.(6)

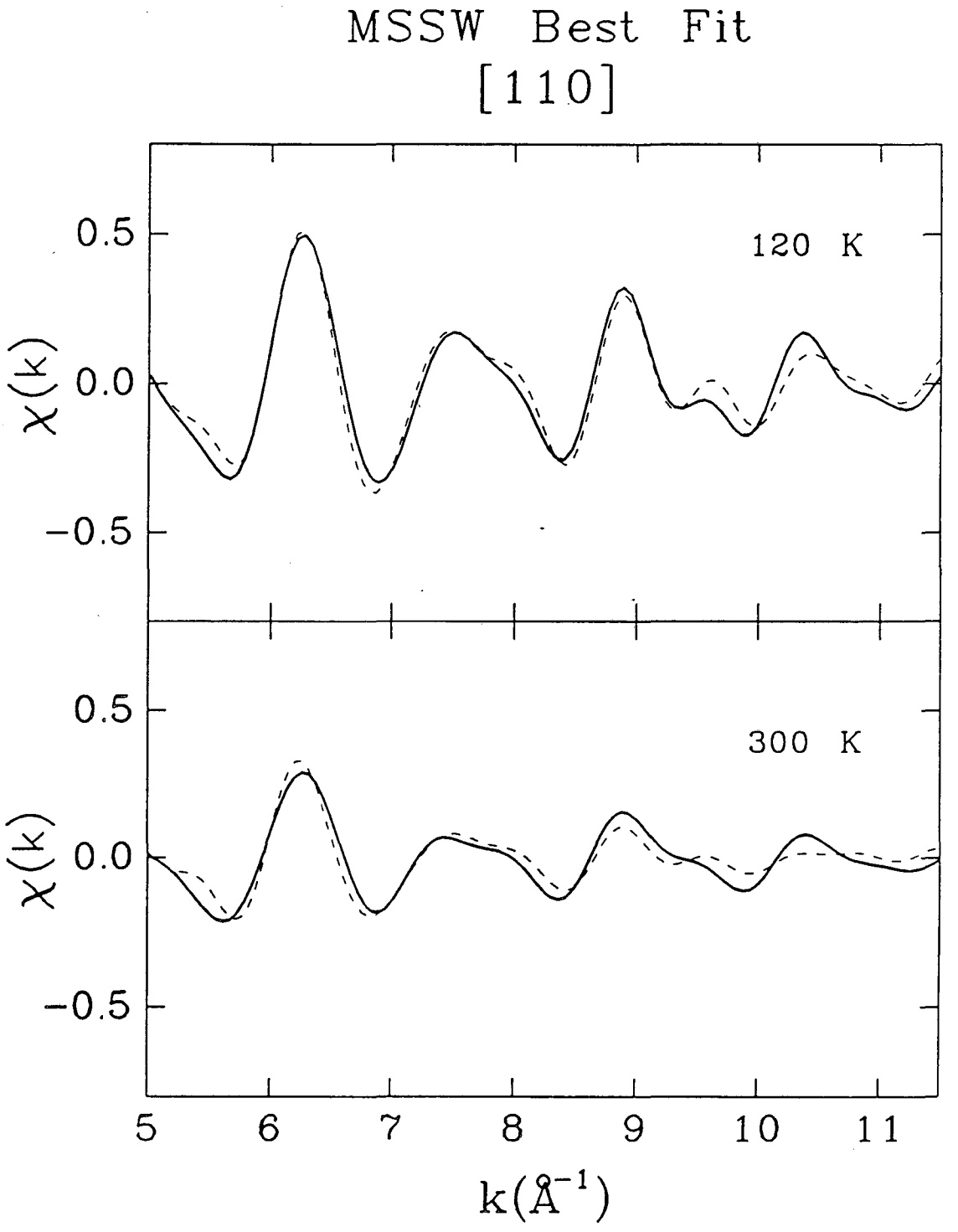

Fig.(7)

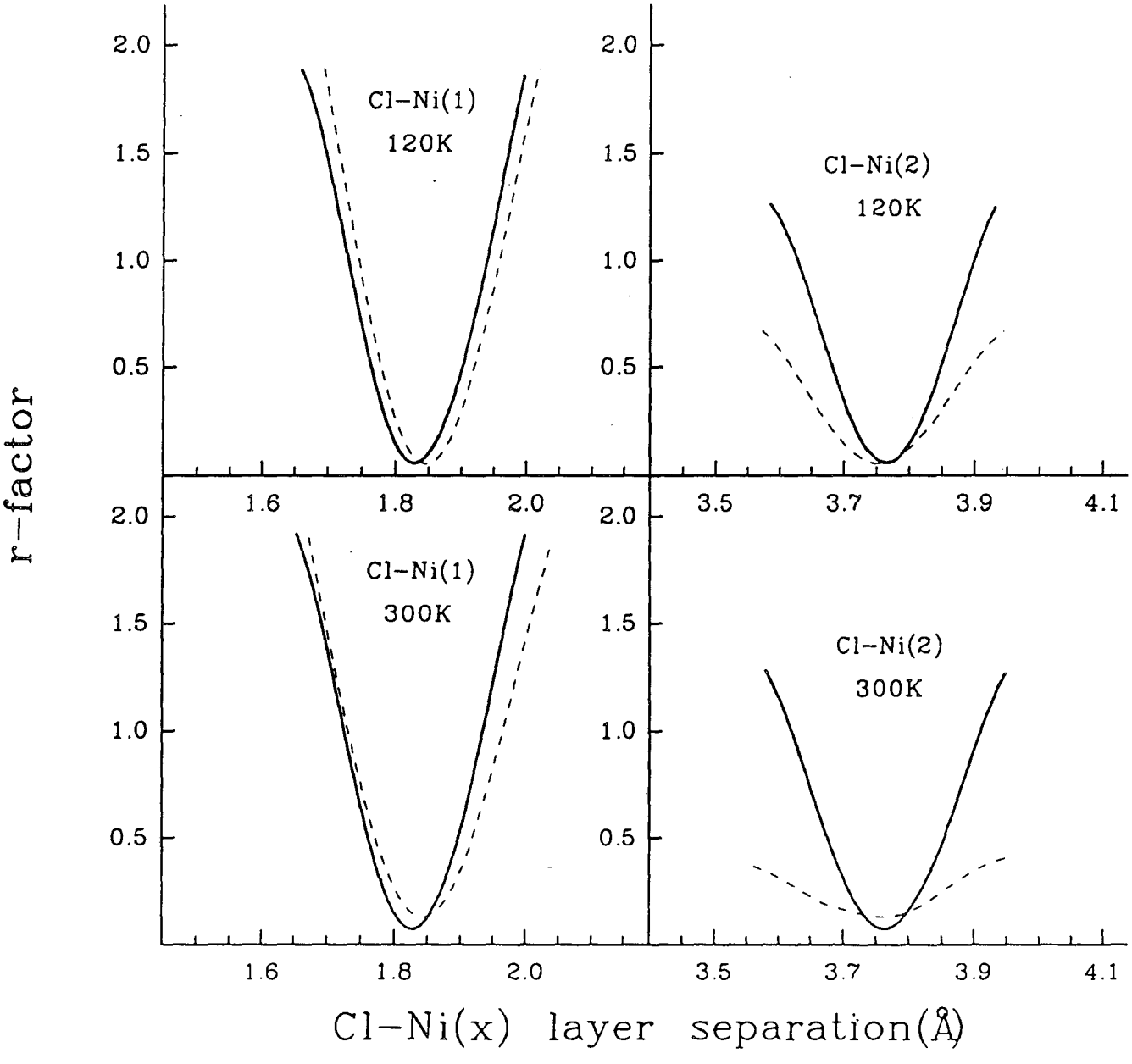
r-factor
2.0
1.5
1.0
0.5
Cl-Ni(1)
120K
Cl-Ni(2)
120K
Cl-Ni(1)
300K
Cl-Ni(2)
300K
1.6
1.8
2.0
3.5
3.7
3.9
4.1
Cl-Ni(x) layer separation(Å)

Fig.(8)

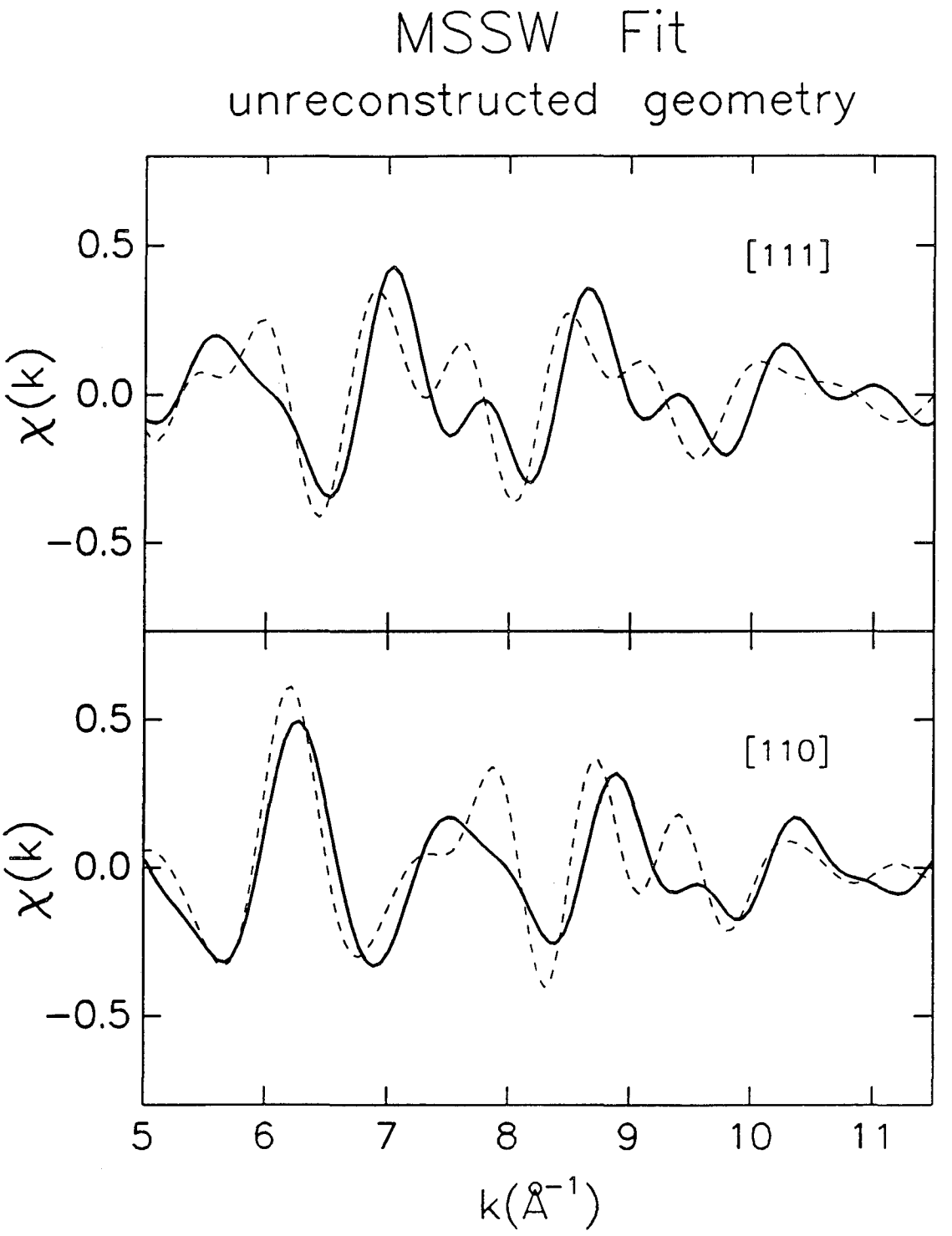
MSSW Fit
unreconstructed geometry
[111]
[110]
χ(k)
0.5
0.0
−0.5
5
6
7
8
9
10
11
k(Å⁻¹)

Fig.(9)

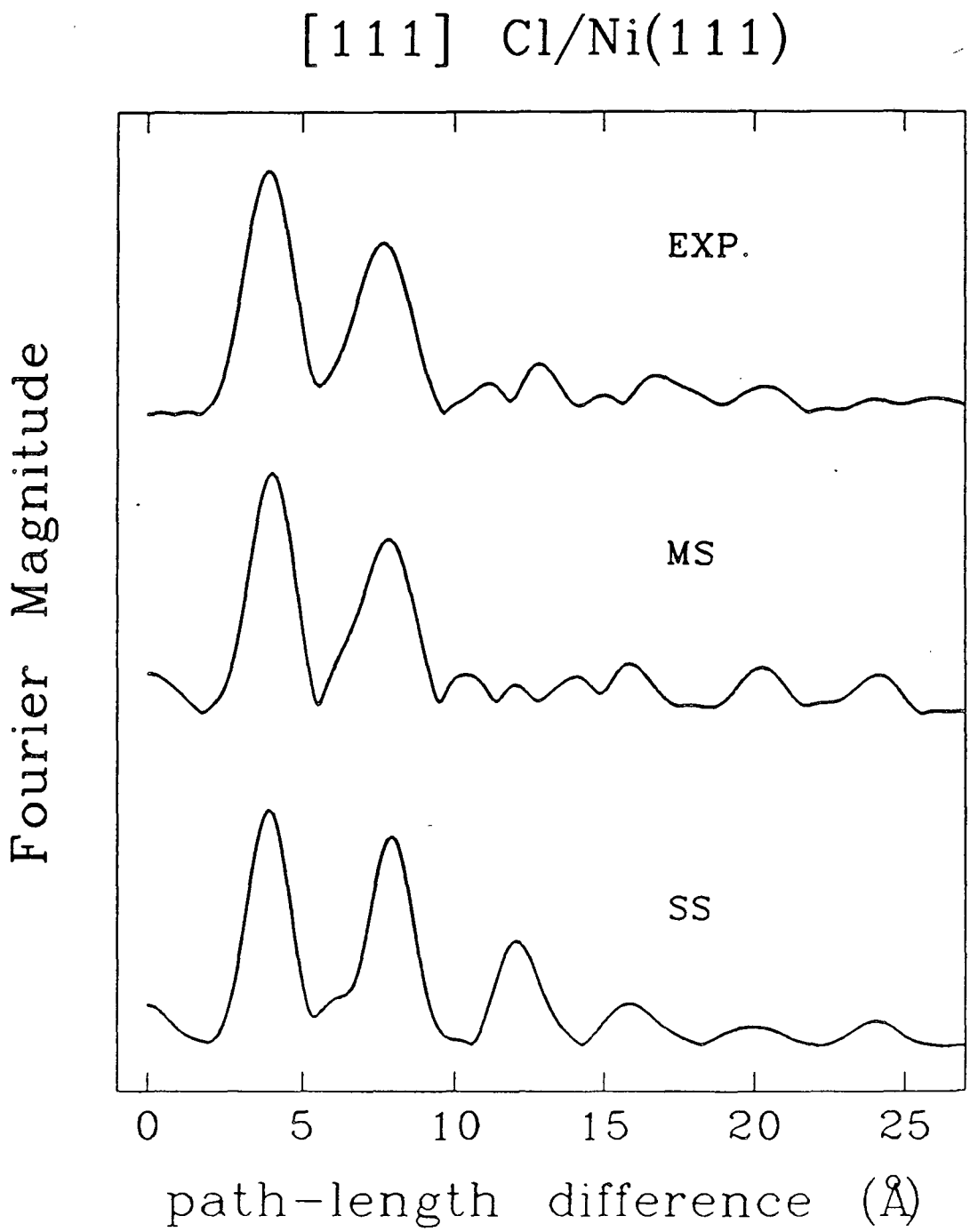
[111] Cl/Ni(111)
EXP.
MS
SS
Fourier Magnitude
0
5
10
15
20
25
path-length difference (Å)

Fig.(10)

LAWRENCE BERKELEY LABORATORY
UNIVERSITY OF CALIFORNIA
INFORMATION RESOURCES DEPARTMENT
BERKELEY, CALIFORNIA 94720